Electronic Supplementary Material (ESI) for Chemical Communications.

A high performance tungsten bronze electrode in a mixed electrolyte and applications in supercapacitors

Zhen Sun,[a] Xiao-Guang Sang,[a] Yu Song,[a] Di Guo,[a] Dong-Yang Feng,[a] Xiaoqi Sun,*[a] Xiao-Xia Liu*[a,b]

[a]Department of Chemistry, Northeastern University, Shenyang, 110819, China

[b]Key Laboratory of Data Analytics and Optimization for Smart Industry (Northeastern University), Ministry of Education, Shenyang, 110819, China

Corresponding authors: Xiaoqi Sun, sunxiaoqi@mail.neu.edu.cn

Xiao-Xia Liu, xxliu@mail.neu.edu.cn

1. Experimental Sections

1.1 Materials

All the reagents were purchased from Sinopharm Chemical Reagent Co., Ltd. (China) and used as received. Carbon cloth and graphite foil were purchased from Fuel Cell Earth (United States) and SGL group (Germany), respectively.

1.2 Fabrication of tungsten bronze on carbon cloth

The synthesis was carried out in a three-electrode electrochemical cell, using saturated calomel electrode (SCE) as the reference electrode and graphite foil as the counter electrode. Tungsten oxide was electrodeposited on carbon cloth (1×1 cm^2) by a constant potential hold at −1.0 V for 1 h in the aqueous mixture of 0.01 M sodium tungstate, 0.01 M hydrochloric acid and 0.04 M hydrogen peroxide. The obtained electrode was further electro-crystallized by cyclic voltammetry (CV) in the potential range of −0.5 ~ 0 V at the scan rate of 100 mV s^{-1} in 1 M H_2SO_4. The tungsten bronze electrode was obtained after 50 k cycles. The loading of tungsten bronze active material was 6 mg cm^{-2}.

1.3 Assembly of asymmetric supercapacitors

The ASC device was assembled by using tungsten bronze and reduced exfoliated graphite (REG) as the anode and cathode, respectively. The REG cathode was obtained by electrochemical treatments of graphite foil (1×1 cm^2) in three-electrode systems using platinum plate and SCE as the counter and reference electrode, respectively. The graphite foil was treated by CV scans from 0.6 to 1.8 V at 20 mV s^{-1} in the 0.5 M K_2CO_3 solution for 7 cycles, followed by the constant potential hold at 1.8 V for 2 h in 0.5 M KOH. The electrical conductivity of the electrode was finally recovered by CV scans from −0.9 to 1 V for 60 cycles at 50 mV s^{-1} in 3 M KCl solution. To assemble the ASC device, a piece of

separator (NKK separator, Japan) was soaked in the 1 M Na_2SO_4 + 0.01 M H_2SO_4 electrolyte and sandwiched between the two electrodes. The device was finally sealed by parafilm.

1.4 Characterization

The morphologies of electrode materials were investigated by scanning electron microscopy (SEM, Ultra Plus, Carl Zeiss, Germany). The crystal structures were characterized by X-ray diffraction (XRD, X'Pert Pro, PANalytical B.V., Netherlands). The chemical composites and oxidation states of the samples were examined by X-ray photoelectron spectroscopy (XPS, ESCALAB 250Xi, Thermo Scientific Escalab, USA). The surface area of the materials was measured by the Brunauer–Emmett–Teller (BET) method using an ASAP 2460 (MicroActive, USA). Electrochemical measurements were conducted on a multichannel electrochemical analyzer (VMP3, Bio-Logic-Science Instruments, France). The mass loading of active materials was measured with a Sartorius BT 25 S semi-microbalance with the accuracy of 0.01 mg.

2. Calculations

2.1 Single electrode

Areal capacitance (C_a) of the single electrode can be calculated from the CV curves using the following Equation S1:

$$C_a = \frac{\int IdU}{2v\Delta U} = \frac{S}{2v\Delta U} \qquad \text{(Equation S1)}$$

where v is the scan rate, S is the area of the closed CV curve, ΔU is the potential window. The area of the active material was controlled to be 1 cm^2.

2.2 Device

Volumetric capacitance (C_v) of ASC device is calculated from the galvanostatic charge-discharge profiles by the following Equation S2:

$$C_v = \frac{It}{VU} \qquad \text{(Equation S2)}$$

Where I is the discharge current, t is the discharge time, V is the volume and U is the voltage window of the ASC. The volume of the device was 0.055 cm^3.

Volumetric energy density and power density are calculated according to Equation S3 and S4:

$$E_v = \frac{C_v U^2}{2 \times 3.6} \qquad \text{(Equation S3)}$$

$$P_v = \frac{3600E_v}{t} \qquad \text{(Equation S4)}$$

where E_v is volumetric energy densities, P_v is the volumetric power densities, C_v is the volumetric capacitance, t is the discharge time and U is the voltage window of the device.

2.3 Discussion on the charge storage mechanism

The charge storage mechanisms of the tungsten bronze electrode were studied. The scan rate v and current density i in CV obey the relationship below:

$$i = av^b \qquad \text{(Equation S5)}$$

where a and b are variable values. The b value is obtained from the slope of the log(i) versus log(v) plot. A b-value close to 1 suggests a capacitive nature while b close to 0.5 indicates a diffusion-controlled process. The b-values of the tungsten bronze electrode were calculated at different potentials and all show larger than 0.8 values (Fig. S6a), demonstrating a high capacitive contribution for charge storage. The detailed capacitive and diffusion controlled contributions were obtained according to the following equation：

$$i = k_1v + k_2v^{1/2} \qquad \text{(Equation S6)}$$

with k_1 and k_2 representing capacitive and diffusion controlled coefficients, respectively. The obtained percentages are summarized in Fig. S6b. The percent of capacitive contribution increases with scan rates, from 56% at 1 mV s^{-1} to 90% at 20 mV s^{-1}. The high capacitive contribution is ascribed to the short ion diffusion path and rapid electron transfer in the interconnected nano-sheets, which is also essential for the excellent rate capability of the tungsten bronze electrode.

3. Supplementary figures

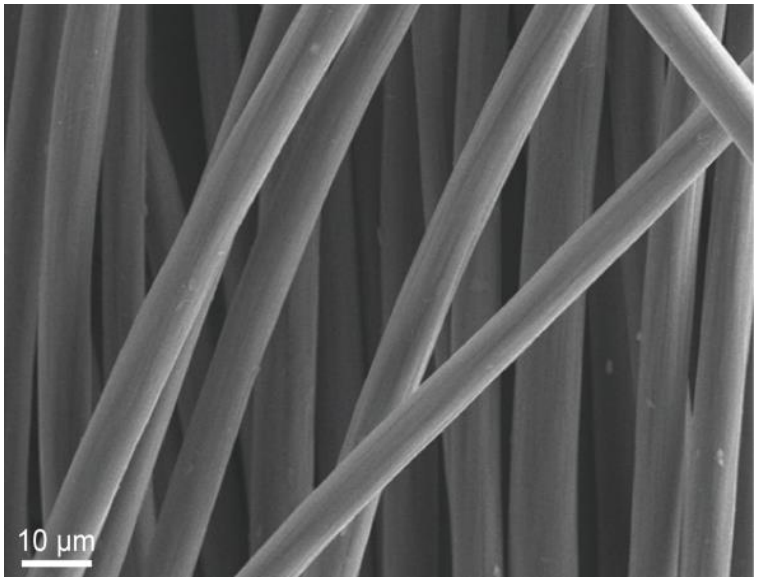

Fig. S1 SEM image of carbon cloth.

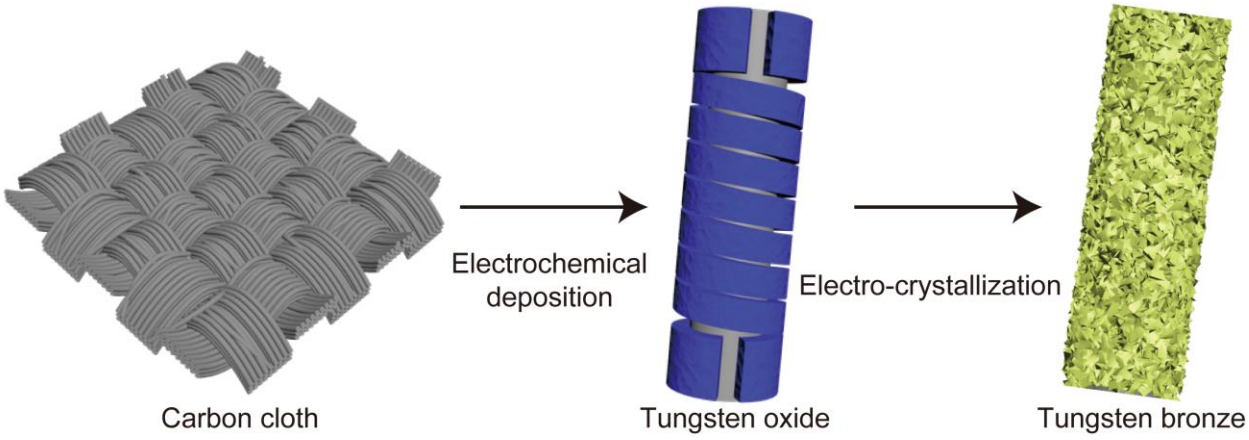

Fig. S2 Schematic diagram of the synthesis process of tungsten bronze on carbon cloth.

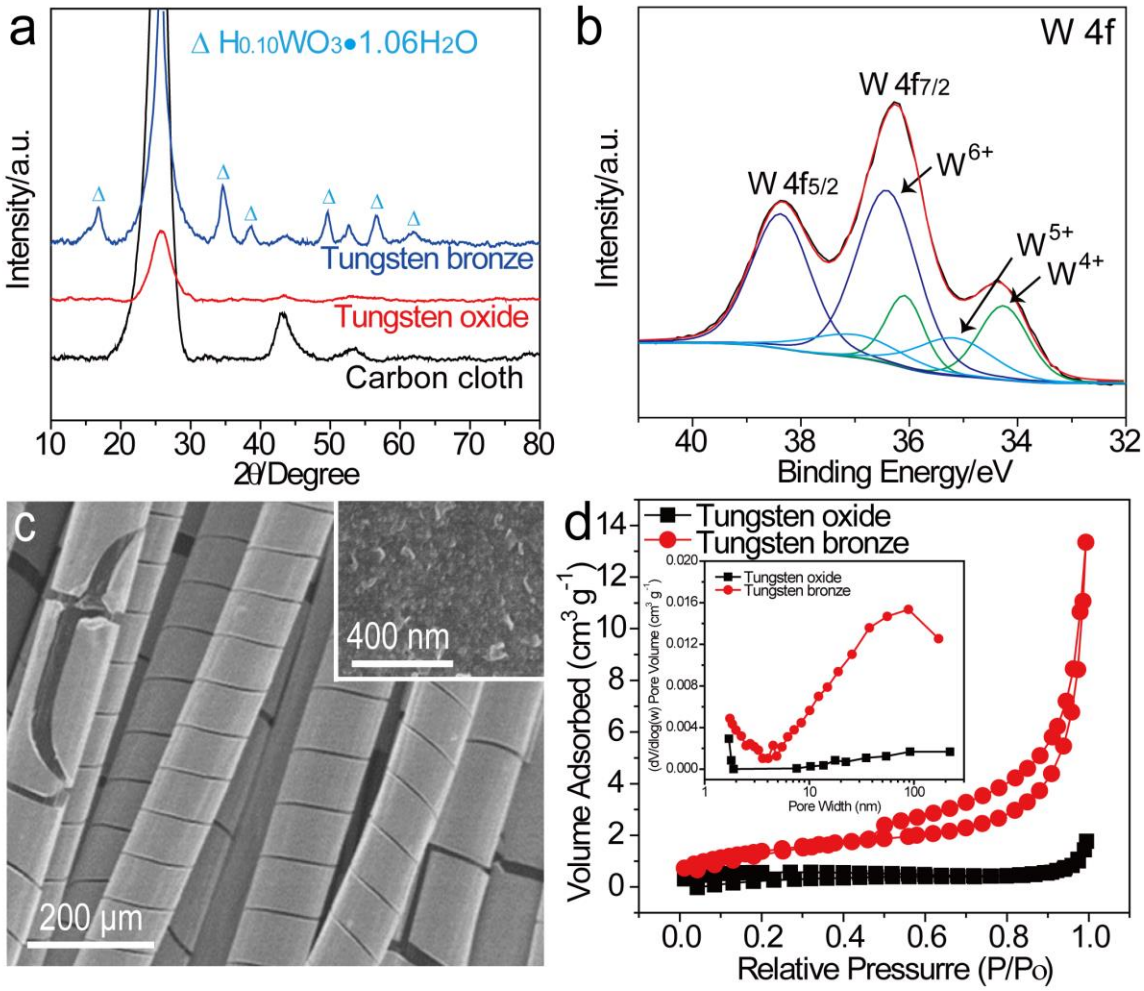

Fig. S3. (a) XRD patterns of the as-prepared tungsten oxide, electro-crystallized tungsten bronze and carbon cloth. (b) W 4f XPS fitting and (c) SEM images of the as-prepared tungsten oxide (the inset shows the high-magnification image). (d) N_2 adsorption−desorption isotherms for the as-prepared tungsten oxide and electro-crystallized tungsten bronze electrodes (the inset shows the pore size distributions).

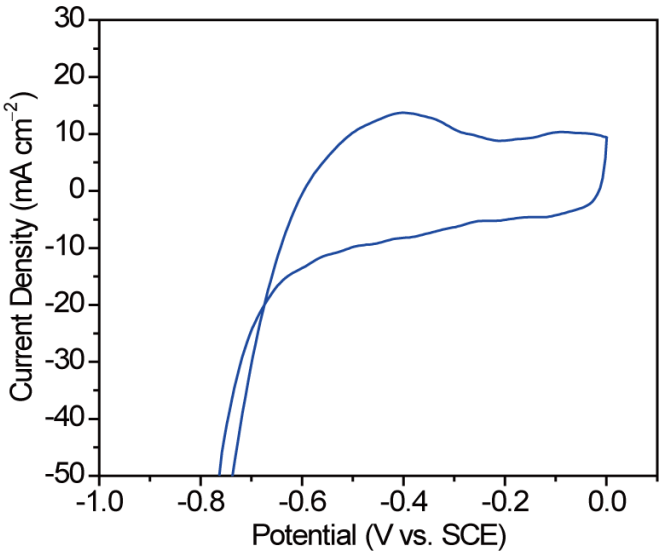

Fig. S4 CV curve of the tungsten bronze electrode in 1 M H_2SO_4 at the scan rate of 5 mV s^{-1}.

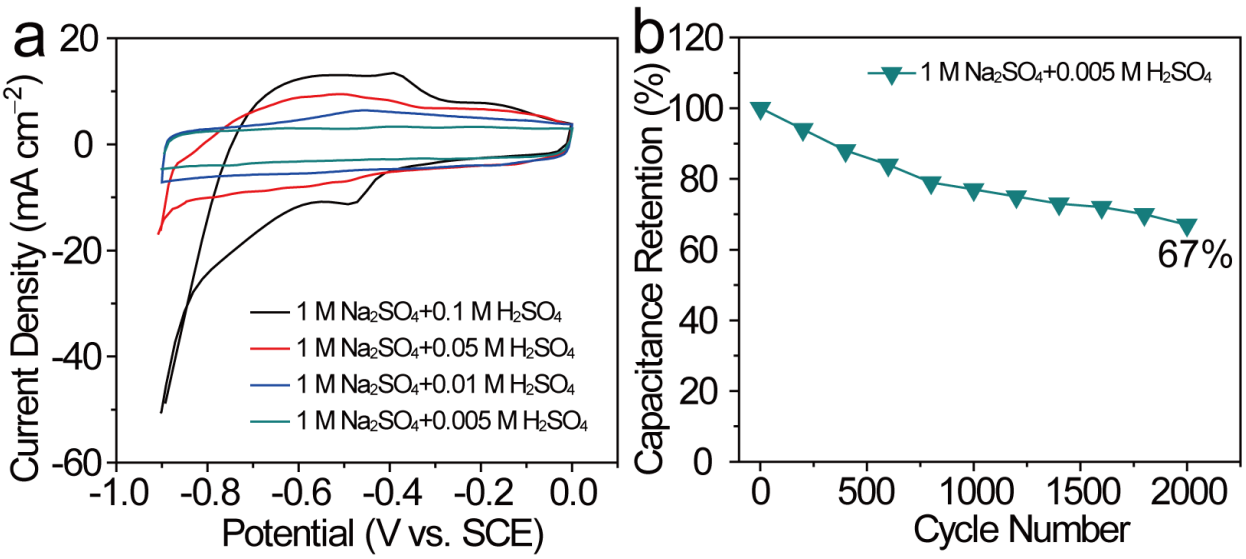

Fig. S5 (a) CV curves of tungsten bronze in 1 M Na_2SO_4 and various amount of H_2SO_4. (b) Cycling performance of tungsten bronze in the mixed electrolyte of 1 M Na_2SO_4 + 0.005 M H_2SO_4.

Among various electrolyte compositions, the 1 M Na_2SO_4 + 0.01 M H_2SO_4 electrolyte shows optimal performance. It provides a stable potential window of –0.9 V to 0 V (*vs.* SCE) for the tungsten bronze electrode, while hydrogen evolution reaction (HER) starts at around –0.85 V in the case of 1 M Na_2SO_4 + 0.05 M H_2SO_4 (Fig. S5a). Further increase of H_2SO_4 concentration results in even earlier HER and thus smaller potential window. On the other hand, when decreasing the H_2SO_4 concentration to 0.005 M, the –0.9 V to 0 V potential window is preserved. However, the tungsten bronze electrode delivers smaller capacitance and much poorer cycling life. Only 67% capacitance is retained after 2000 cycles (Fig. S5b), in direct contrast to the ultra-stable cycle life in 1 M Na_2SO_4 + 0.01 M H_2SO_4 for over 30 000 cycles (Fig. 2c). It is presumably due to the ineffective inhibition of phase transformation of tungsten bronze with not enough proton addition.

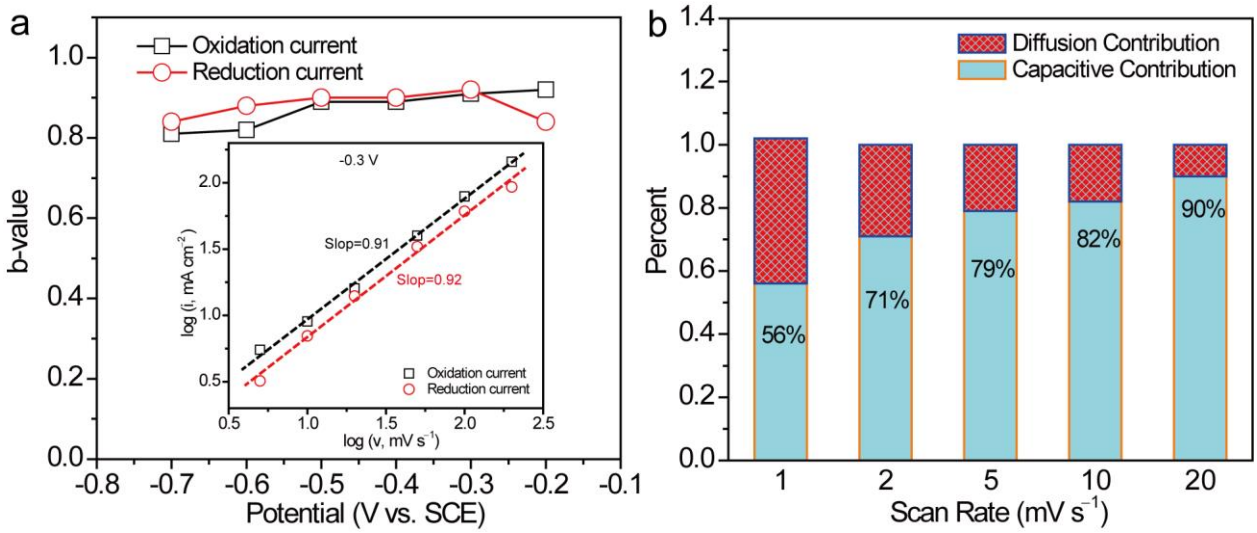

Fig. S6 (a) *b* values at selected potentials (the inset shows the plot of log(*i*) *vs*. log(*v*) at –0.3 V). (b) Percentage of capacitance contribution at different scan rates.

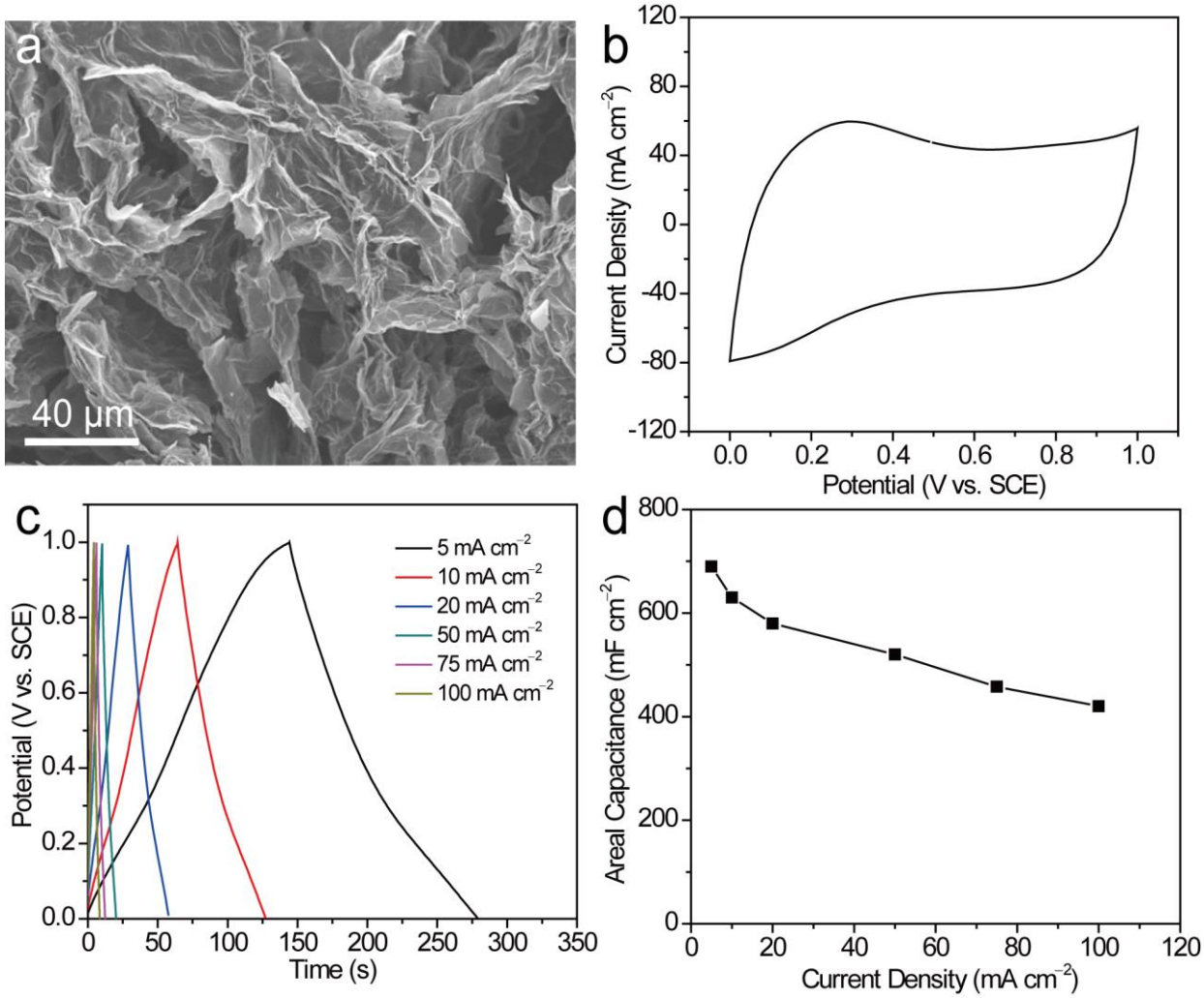

Fig. S7 (a) SEM image of REG. (b) CV of REG at 100 mV s^{-1}. (c) Galvanostatic charge-discharge curves of the REG electrode. (d) Areal capacitance of REG at different current densities.

Fig. S7a shows the SEM image of the REG. The nanosheet morphology provides abundant open space. The electrochemical performance of the REG electrode was investigated in three electrode systems. Fig. S7b and c shows the CV and galvanostatic charge-discharge curves of the electrode in the 1 M Na_2SO_4 + 0.01 M H_2SO_4 mixed electrolytes. REG delivers an areal capacitance of 690 mF cm^{-2} at 5 mA cm^{-2}, and 60% capacitance is retained when the current density increases to 100 mA cm^{-2} (Fig. S7d).

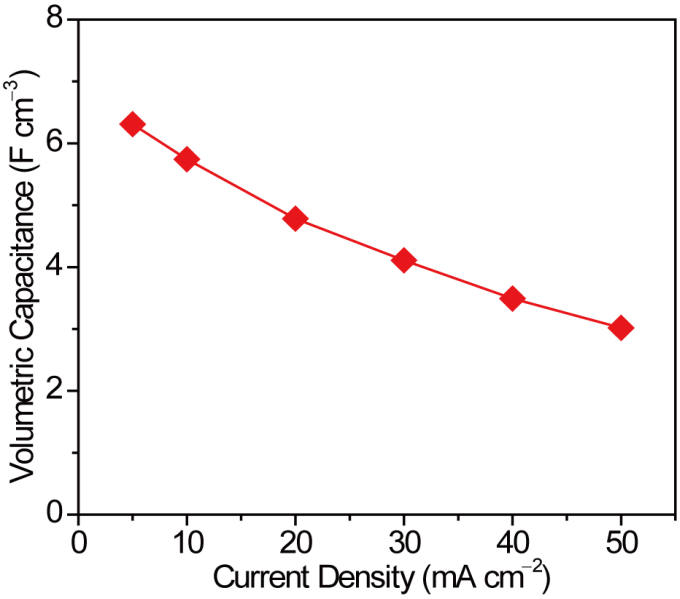

Fig. S8 Volumetric capacitance of the ASC device at different current densities.

4. Supplementary table

Table S1. Electrochemical performance comparison of tungsten-based pseudocapacitive electrodes.

Material	Potential Window	Electrolyte	Capacitance	Cycling Stability
NFL-WO_3[S1]	–0.5 ~ 0 V (Ag/AgCl)	1 M H_2SO_4	658 mF/cm^2 @6 mA/cm^2 196 F/g@10 mV/s	85% after 5000 cycles
WO_3[S2]	–0.35 ~ 0.2 V (SCE)	2 M H_2SO_4	797.05 F/g@0.5 A/g 872.73 F/g@10 mV/s	100.47% after 2000 cycles
WO_3[S3]	–0.6 ~ 0 V (Ag/AgCl)	1 M H_2SO_4	403.5 F/g@5 mV/s	N/A
h-WO_3[S4]	–0.5 ~ 0 V (SCE)	0.5 M H_2SO_4	417.8 F/g@2 mV/s 421.8 F/g@0.5 A/g	100% after 1000 cycles
WO_3[S5]	–0.6 ~ 0 V (Ag/AgCl)	1 M H_2SO_4	102.4 mF/cm^2 @10 mV/s	N/A
WO_3–WO_3·0.5H_2O[S6]	–0.6 ~ 0.2 V (Ag/AgCl)	0.5 M H_2SO_4	290 F/g@25 mV/s	N/A
WO_3[S7]	–0.6 ~ 0 V (Ag/AgCl)	1 M H_2SO_4	53 mF/cm^2 @1 mA/cm^2	81% after 4000 cycles
WO_3[S8]	–0.6 ~ 0 V (Ag/AgCl)	1 M H_2SO_4	13.6 mF/cm^2 @10 mV/s	72.6% after 5000 cycles
WO_3[S9]	–0.65 ~ 0.2 V (SCE)	1 M H_2SO_4	385 F/g@0.5 A/g	N/A
WO_3[S10]	–0.7 ~ 0 V (Ag/AgCl)	0.5 M H_2SO_4	2575.3 F/cm^2 @3 mA/cm^2 643.9 F/g@0.75 A/g	85.1% after 6000 cycles

Table S1. Electrochemical performance comparison of tungsten-based pseudocapacitive electrodes (continued).

Material	Potential Window	Electrolyte	Capacitance	Cycling Stability
$W_{18}O_{49}$[S11]	–0.6 ~ 0.2 V (Ag/AgCl)	1 M H_2SO_4	440 F/g@2 A/g	N/A
WO_3[S12]	–0.5 ~ 0 V (SCE)	1 M H_2SO_4	694 F/g@0.35 A/g 404 F/g@5 mV/s	87% after 2000 cycles
LC-WO_3[S13]	–0.5 ~ 0.2 V (SCE)	1M H_2SO_4	200 mF/cm^2@0.1 A/g	N/A
h-WO_3/SWCNT[S14]	–0.5 ~ 0.3 V (Ag/AgCl)	1 M H_2SO_4	510 F/g@2 mV/s	87% after 5000 cycles
h-WO_3·nH_2O/CNT[S15]	–0.6 ~ 0.3 V (Ag/AgCl)	0.2 M H_2SO_4	498 F/g@5 mV/s	100% after 50 000 cycles
WO_3/WNCC[S16]	–0.6 ~ 0.3 V (Ag/AgCl)	2 M H_2SO_4	680 F/g@0.5 A/g	100% after 2000 cycles
graphene-WO_3[S17]	–0.4 ~ 0.6 V (SCE)	0.1 M H_2SO_4	465 F/g@1 A/g 980 F/g@1 mV/s	97.7% after 2000 cycles
WO_3 NRs/rGO[S18]	–0.6 ~ 0.1 V (Ag/AgCl)	0.5 M H_2SO_4	343 F/g@0.2 A/g	92.7% after 1000 cycles
$H_{0.12}WO_3$·H_2O[S19]	–0.55 ~ 0.1 V (SCE)	0.5 M H_2SO_4	5.95 F/cm^2 @2 mA/cm^2	100% after 5000 cycles
e-WO_3[S20]	–0.5 ~ 0 V (SCE)	0.5 M H_2SO_4	10m F/cm^2 @0.05 mA/cm^2	N/A
m-WO_{3-x}-C-s[S21]	–0.2 ~ 0.8 V (Ag/AgCl)	2 M H_2SO_4	103 F/g@1 m V/s	N/A
WO_{3-x}[S22]	–0.1 ~ 0.8 V (SCE)	2 M H_2SO_4	199 F/g@1 mA/cm^2	N/A

Table S1. Electrochemical performance comparison of tungsten-based pseudocapacitive electrodes (continued).

Material	Potential Window	Electrolyte	Capacitance	Cycling Stability
WO_3/CA[S23]	–0.3 ~ 0.5 V (Ag/AgCl)	0.5 M H_2SO_4	700 F/g@25 mV/s	95% after 4000 cycles
$WO_3 \cdot H_2O$[S24]	–0.3 ~ 0.15 V (Ag/AgCl)	0.05 M H_2SO_4	39.7 F/cm^2 @0.07 mA/cm^2	N/A
$OMC/WO_{2.83}$[S25]	–0.2 ~ 0.4 V (SCE)	1 M H_2SO_4	175 F/g@2 mV/s	113% after 1000 cycles
WO_3/CA[S26]	–0.3 ~ 0.5 V (Ag/AgCl)	2 M H_2SO_4	609 F/g@5 mV/s	98% after 1000 cycles
WO_3/C[S27]	–0.4 ~ 0.2 V (Ag/AgCl)	0.5 M H_2SO_4	508 F/g@1 A/g	97% after 1000 cycles
WO_3[S28]	–0.6 ~ 1.0 V (Ag/AgCl)	0.5 M H_2SO_4	169 F/g@2 A/g	N/A
nc-WO_3/C[S29]	–0.3 ~ 0.2 V (Ag/AgCl)	0.5 M H_2SO_4	702 F/g@2 mV/s	110.2% after 4000 cycles
h-WO_3[S30]	–0.3 ~ 0.6 V (Ag/AgCl)	0.5 M H_2SO_4	15.6 mF/cm^2@5 mV/s	N/A
WO_3/ZnO[S31]	–0.9 ~ 0 V (Ag/AgCl)	1 M $LiClO_4$	15.24 mF/cm^2 @0.14 mA/cm^2	N/A
C@WO_{3-x} CF[S32]	–1 ~ 0 V (SCE)	5 M LiCl	786.8 mF/cm^2 @20 mA/cm^2	87.7% after 10 000 cycles
WO_3[S33]	–0.7 ~ 0.4 V (SCE)	1 M Na_2SO_4	21.4 mF/cm^2 @10 mV/s	N/A
MoO_{3-x}/WO_{3-x}[S34]	–1.1 ~ 0 V (Ag/AgCl)	0.5 M Na_2SO_4	500 mF/cm^2 @2 mA/cm^2	N/A

Table S1. Electrochemical performance comparison of tungsten-based pseudocapacitive electrodes (continued).

Material	Potential Window	Electrolyte	Capacitance	Cycling Stability
H_xWO_{3-y}/NCC[S35]	–1 ~ 1.0 V (SCE)	5 M LiCl	676 F/g (1352 mF/cm^2) @5 mA/cm^2	N/A
WO_{3-x}/CC[S36]	–1 ~ 0 V (SCE)	5 M LiCl	1830 mF/cm^2 @1 mA/cm^2	74.8% after 10 000 cycles
This work	**–0.9 ~ 0 V (SCE)**	**1 M Na_2SO_4 + 0.01 M H_2SO_4**	**860 mF/cm^2 @5 mA/cm^2**	**98% after 30 000 cycles**

References

S1. M. Qiu, P. Sun, L. Shen, K. Wang, S. Song, X. Yu, S. Tan, C. Zhao and W. Mai, *J. Mater. Chem. A*, 2016, **4**, 7266-7273.

S2. J. Xu, T. Ding, J. Wang, J. Zhang, S. Wang, C. Chen, Y. Fang, Z. Wu, K. Huo and J. Dai, *Electrochim. Acta*, 2015, **174**, 728-734.

S3. P. Yang, P. Sun, L. Du, Z. Liang, W. Xie, X. Cai, L. Huang, S. Tan and W. Mai, *J. Phys. Chem. C*, 2015, **119**, 16483-16489.

S4. M. Zhu, W. Meng, Y. Huang, Y. Huang and C. Zhi, *ACS Appl. Mater. Interfaces*, 2014, **6**, 18901-18910.

S5. P. Yang, P. Sun, Z. Chai, L. Huang, X. Cai, S. Tan, J. Song and W. Mai, *Angew. Chem. Int. Ed.*, 2014, **53**, 11935-11939.

S6. K.-H. Chang, C.-C. Hu, C.-M. Huang, Y.-L. Liu and C.-I. Chang, *J. Power Sources*, 2011, **196**, 2387-2392.

S7. Y. Zhong, Z. Chai, Z. Liang, P. Sun, W. Xie, C. Zhao and W. Mai, *ACS Appl. Mater. Interfaces*, 2017, **9**, 34085-34092.

S8. L. Shen, L. Du, S. Tan, Z. Zang, C. Zhao and W. Mai, *Chem. Commun.*, 2016, **52**, 6296-6299.

S9. H. Peng, G. Ma, K. Sun, J. Mu, M. Luo and Z. Lei, *Electrochim. Acta*, 2014, **147**, 54-61.

S10. X. Wu and S. Yao, *Nano Energy*, 2017, **42**, 143-150.

S11. Y. Tian, S. Cong, W. Su, H. Chen, Q. Li, F. Geng and Z. Zhao, *Nano Lett.*, 2014, **14**, 2150-2156.

S12. P. A. Shinde, A. C. Lokhande, N. R. Chodankar, A. M. Patil, J. H. Kim and C. D. Lokhande, *Electrochim. Acta*, 2017, **224**, 397-404.

S13. J. Chen, H. Wang, J. Deng, C. Xu and Y. Wang, *J. Mater. Chem. A*, 2018, **6**, 8986-8991.

S14. W. Sun, M. T. Yeung, A. T. Lech, C. W. Lin, C. Lee, T. Li, X. Duan, J. Zhou and R. B. Kaner,

Nano Lett., 2015, **15**, 4834-4838.
S15. Z. Chen, Y. Peng, F. Liu, Z. Le, J. Zhu, G. Shen, D. Zhang, M. Wen, S. Xiao, C. P. Liu, Y. Lu and H. Li, *Nano Lett.*, 2015, **15**, 6802-6808.
S16. L. Gao, X. Wang, Z. Xie, W. Song, L. Wang, X. Wu, F. Qu, D. Chen and G. Shen, *J. Mater. Chem. A*, 2013, **1**, 7167-7173.
S17. A. K. Nayak, A. K. Das and D. Pradhan, *ACS Sustainable Chem. Eng.*, 2017, **5**, 10128-10138.
S18. X.-h. Guan, Z.-w. Zhang, L. Yang and G.-s. Wang, *ChemPlusChem*, 2017, **82**, 1174-1181.
S19. G. Yang and X.-X. Liu, *J. Power Sources*, 2018, **383**, 17-23.
S20. M. Zhu, Y. Huang, Y. Huang, W. Meng, Q. Gong, G. Li and C. Zhi, *J. Mater. Chem. A*, 2015, **3**, 21321-21327.
S21. C. Jo, J. Hwang, H. Song, A. H. Dao, Y.-T. Kim, S. H. Lee, S. W. Hong, S. Yoon and J. Lee, *Adv. Funct. Mater.*, 2013, **23**, 3747-3754.
S22. S. Yoon, E. Kang, J. K. Kim, C. W. Lee and J. Lee, *Chem. Commun.*, 2011, **47**, 1021-1023.
S23. Y.-H. Wang, C.-C. Wang, W.-Y. Cheng and S.-Y. Lu, *Carbon*, 2014, **69**, 287-293.
S24. H. Farsi, F. Gobal and Z. Barzgari, *Ionics*, 2012, **19**, 287-294.
S25. Y. Zhou, S. Ko, C. W. Lee, S. G. Pyo, S.-K. Kim and S. Yoon, *J. Power Sources*, 2013, **244**, 777-782.
S26. X. Liu, G. Sheng, M. Zhong and X. Zhou, *Nanoscale*, 2018, **10**, 4209-4217.
S27. D. Mandal, P. Routh and A. K. Nandi, *Small*, 2018, **14**, 1702881.
S28. W. Q. Wang, X. L. Wang, X. H. Xia, Z. J. Yao, Y. Zhong and J. P. Tu, *Nanoscale*, 2018, **10**, 8162-8169.
S29. J. Jia, X. Liu, R. Mi, N. Liu, Z. Xiong, L. Yuan, C. Wang, G. Sheng, L. Cao, X. Zhou and X. Liu, *J. Mater. Chem. A*, 2018, **6**, 15330-15339.
S30. M. Zhu, Y. Huang, Y. Huang, Z. Pei, Q. Xue, H. Li, H. Geng and C. Zhi, *Adv. Funct. Mater.*, 2016, **26**, 4481-4490.
S31. Z. Bi, X. Li, Y. Chen, X. Xu, S. Zhang and Q. Zhu, *Electrochim. Acta*, 2017, **227**, 61-68.
S32. C. Yao, B. Wei, H. Li, G. Wang, Q. Han, H. Ma and Q. Gong, *J. Mater. Chem. A*, 2017, **5**, 56-61.
S33. N. M. Shinde, A. D. Jagadale, V. S. Kumbhar, T. R. Rana, J. Kim and C. D. Lokhande, *Korean J. Chem. Eng.*, 2015, **32**, 974-979.
S34. X. Xiao, T. Ding, L. Yuan, Y. Shen, Q. Zhong, X. Zhang, Y. Cao, B. Hu, T. Zhai, L. Gong, J. Chen, Y. Tong, J. Zhou and Z. L. Wang, *Adv. Energy Mater.*, 2012, **2**, 1328-1332.
S35. H. Wang, R. Fan, J. Miao, J. Chen, S. Mao, J. Deng and Y. Wang, *J. Mater. Chem. A*, 2018, **6**, 6780-6784.
S36. R. Wang, Y. Lu, L. Zhou, Y. Han, J. Ye, W. Xu and X. Lu, *Electrochim. Acta*, 2018, **283**, 639-645.